PTEP

Prog. Theor. Exp. Phys. **2012**, 04D004 (24 pages)
DOI: 10.1093/ptep/pts073

# Sensitivity to dark energy candidates by searching for four-wave mixing of high-intensity lasers in the vacuum

Kensuke Homma[1,2*]

[1]*Graduate School of Science, Hiroshima University, Kagamiyama, Higashihiroshima, Hiroshima 739-8526, Japan*
[2]*International Center for Zetta-Exawatt Science and Technology, Ecole Polytechnique, Route de Saclay, F-91128 Palaiseau Cedex, France*
[*]E-mail: E-mail: homma@hepl.hiroshima-u.ac.jp

Received September 1, 2012; Accepted November 12, 2012; Published December 17, 2012

Theoretical challenges to understand dark matter and dark energy suggest the existence of low-mass and weakly coupling fields in the universe. The quasi-parallel photon–photon collision system (QPS) can provide chances to probe the resonant production of these light dark fields and the induced decay by the coherent nature of laser fields simultaneously. By focusing high-intensity lasers with different colors in the vacuum, new colors emerge as signatures of the interaction. Because four photons in the initial and final states interact via dark field exchange, this process is analogous to four-wave mixing in quantum optics, where the frequency sum and difference between the incident three waves generate the fourth wave with a new frequency via the nonlinear property of crystals. The interaction rate of the four-wave mixing process has cubic dependence on the intensity of each wave. Therefore, if high-intensity laser fields are given, the sensitivity to the feeble coupling of dark fields to photons rapidly increases over a wide mass range below the sub-eV level. Based on experimentally measurable photon energies and linear polarization states, we formulate a relation between the accessible mass-coupling domains and the high-intensity laser parameters, where the effects of the finite spectrum width of pulse lasers are taken into account. The expected sensitivity suggests that we have the potential to explore interactions at the super-Planckian coupling strength in the sub-eV mass range, if cutting-edge laser technologies are properly combined.



## Introduction

Ordinary matter occupies only ∼4% of the total energy density of the universe. The remaining energies are supposed to be occupied by dark matter (DM) ∼23% and dark energy (DE) ∼73% [1]. In addition to the astronomical observations, directly probing these dark components in terrestrial laboratory experiments plays a crucial role in providing different insights into the true characters of the universe or the structure of the vacuum.

Light (pseudo)scalar fields are now indispensable theoretical tools to try to interpret the cosmological constant $\Lambda$ based on the DE scenario [2]. In reduced Planckian units with $c = \hbar = M_{\rm P}(= (8\pi G)^{-1/2} \sim 10^{27}\,{\rm eV}) = 1$, the observed $\Lambda \sim 10^{-120}$ is extremely small compared to the theoretically natural scale $\Lambda \sim 1$. There is a variety of theoretical models on the market. In order for a DE model to be falsifiable by laboratory experiments, we clarify the following minimum requirements for the model:

- solves the *fine-tuning problem*: how to realize such an extremely small $\Lambda$,
- solves the *coincidence problem*: why the energy density coincides with the matter density only at once at present so accidentally among the long history of the universe,
- predicts the field–matter coupling strength, the mass scale of the exchanged field, and the measurable dynamical effect, e.g., the force-range.

For instance, quintessence approaches [2] are designed to resolve the *fine-tuning* and *coincidence problems* by introducing the decaying behavior of $\Lambda$ based on the potential of a scalar field. However, the potential forms are rather phenomenologically introduced. In a similar way, scalar-tensor theory with $\Lambda$ (STT$\Lambda$) [5], on the other hand, is grounded upon a conformal transformation and the frame of observations, which gives several testable predictions. Therefore, STT$\Lambda$ is one of the DE models satisfying the above requirements simultaneously. The most significant prediction of STT$\Lambda$ is the decaying behavior of $\Lambda \propto t^{-2}$ as a function of time $t$. The present age of the universe is $t_0 \sim 1.37 \times 10^{10}$ year, corresponding to $t_0 \sim 10^{60.2}$ in reduced Planckian units. Thus, the observed $\Lambda$ is naturally understood by the overall decaying behavior, though expecting short-term fluctuations from the dominant behavior [6]. The decaying behavior depends on the conformal frame on which our observations are based. For example, redshift measurements relevant to DE are implicitly based on the common atomic clock between distant points, i.e., on the common elementary particle masses. In order to realize constancy of particle masses, a consistent conformal frame must be favored on which the gravitational constant $G$ looks constant, the expansion rate of the universe is consistent with observation, and $\Lambda$ decays as $t^{-2}$ by keeping particle masses constant[1]. The choice of a conformal frame unavoidably associates a massless Nambu–Goldstone (NG) boson, because it breaks the scale invariance (global conformal symmetry), which is also known as a dilaton. In contrast to the well-known Brans–Dicke model [7], a kind of scalar-tensor theory, the requirement of constancy of particle masses results in coupling of the scalar field with matter, i.e., violation of the weak equivalence principle only via quantum anomaly coupling [5]. Due to this coupling to matter fields, STT$\Lambda$ uniquely predicts an extremely low-mass scalar field as a pseudo NG boson via explicit symmetry breaking by the quantum loop effect in the self-energy. This is similar to a massive pion as a theoretical descendant of an originally massless NG pseudoscalar boson associated with chiral symmetry. The scalar field couples with other matter fields basically as weakly as gravity. The mass scale $m_\phi$, based on a simple one-loop diagram in which light quarks and leptons with a typical mass $m_\mathrm{q} \sim$ MeV couple to the scalar field with gravitational coupling with the strength $\sim M_\mathrm{P}^{-1}$, is given by

$$m_\phi^2 \sim \frac{m_\mathrm{q}^2 M_\mathrm{ssb}^2}{M_\mathrm{P}^2} \sim (10^{-9}\mathrm{eV})^2, \tag{1}$$

where the effective cutoff coming from the super-symmetry-breaking mass-scale $M_\mathrm{ssb} \sim$ TeV is assumed, though allowing a latitude of several orders of magnitude, if $M_\mathrm{ssb}$ is higher than the conventional TeV scale [5]. We note that the uncertainty on the mass range in the DE scenarios is quite large. Quintessence-based scenarios typically argue that the mass is determined from the second derivative of the assumed almost flat potential, resulting in $m \sim 10^{-33}$ eV[2]. On the other hand, $\Lambda \sim (\mathrm{meV})^4$ in natural units intuitively leads to models based on the particle picture [9–14], assuming a mass

[1] A short summary of Ref. [5] is available. For example, see Ref. [8].

[2] It is rather difficult to interpret the mass scale as the actual particle mass, because there are no local minima in the exponentially damping flat potential form.

scale in the meV range via rather complicated assumptions. For example, the axion-inspired models [9–12] share the similarity to STTΛ by introducing the concept of pseudo NG boson driven by two dominant scales, $M_{\rm P}$ and a scale of the assumed symmetry breaking at a lower energy than $M_{\rm P}$[3].

The finite mass of the scalar field in STTΛ causes non-Newtonian force [15] via the Yukawa potential, also known as the fifth force. The inverse of Eq. (1) gives a finite range corresponding to $\sim$100 m of the force mediated by the exchange of a quantum $\phi$ between local objects. This is an entirely different aspect from the role of a cosmological fluid in accelerating the universe. The force-range was not explicit in the other theoretical models. This unique aspect triggered the past experimental efforts to measure deviations from the Newtonian potential between massive test bodies [16] in different contexts from DE at that time. These measurements, however, are accompanied by large systematic uncertainties due to the uncontrollable macroscopic probes. As an alternative approach, we have proposed the utilization of the nature of high-intensity laser fields toward a laboratory search for the scalar field predicted by STTΛ [17] as an ultimate goal of laboratory experiments.

Furthermore, low-mass and weakly coupling fields are also predicted with a solid foundation in the contexts of particle physics. For example, the axion, a pseudoscalar field, is proposed as a NG boson associated with the global Peccei–Quinn symmetry breaking [18] to naturally maintain the $CP$ conserving nature of the QCD Lagrangian. The axion and invisible axion-like fields have been intensively investigated by astrophysical objects as well as laboratory experiments[4]. Some of them may become cold dark matter candidates, if the mass and the coupling to matter are within the proper range. Such fields may also leave observational isocurvature fluctuations, if symmetry breaking occurs during the inflation phase of the early universe [20,21]. If we can anticipate that the experimental sensitivity reaches the gravitational coupling strength, the detection of such cold dark matter candidates with much stronger couplings to matter naturally comes into view as the preliminary step toward the ultimate goal.

We, therefore, generalized the principle of the measurement to search for both scalar and pseudoscalar fields in a model-independent way as much as possible [22]. As the amplitudes of the laser fields are increased, we can improve the sensitivity to weakly coupling low-mass fields predicted by any types of theories, as long as the coupling to photons is expected. The proposed method can be regarded as a kind of particle collider attempting to produce extremely light resonance states. However, the mass range of interest is, for instance, much lower than that of the Higgs-like boson produced at the Large Hadron Collider (LHC) by more than ten orders of magnitude. In the proposed method, the following two key ingredients to enhance the sensitivity are included.

The first ingredient is the introduction of the quasi-parallel photon–photon collision system (QPS), as illustrated in Fig. 1. This is considered to realize as low a center-of-mass system (CMS) energy as possible between colliding two laser photons for the production of a low-mass field as a resonance state without lowering the incident photon energy below the optical frequency. The head-on collision in CMS corresponds to the case $\vartheta = \pi/2$ in Fig. 3. The quasi-parallel system can be obtained by introducing a Lorentz boost of the head-on collision into the perpendicular direction with respect to the incident direction in CMS. The CMS energy $E_{\rm cms}$ is then expressed as $E_{\rm cms} = 2\omega \sin\vartheta$ with the incident energy of the photon $\omega$. If a small $\vartheta$ is realized in the laboratory frame, it provides an extremely low CMS energy. This is the essence of the introduction of QPS. Moreover, fortunately,

[3] These models, however, tend to fall into a kind of fine-tuning via complicated theoretical assumptions by respecting the energy density too much at present.

[4] For example, see Fig. 2 and Sect. 4 in Ref. [19].

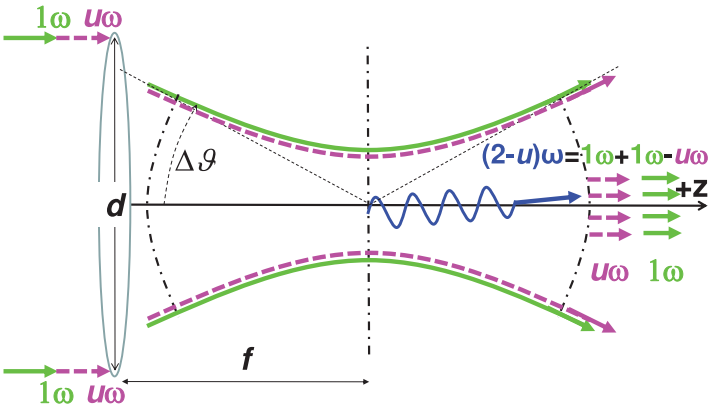


**Fig. 1.** Quasi-parallel colliding system (QPS) between two incident photons out of a focused laser beam with a focal length $f$, a beam diameter $d$, and an upper range of incident angles $\Delta\vartheta$ determined by geometric optics. The signature $(2-u)\omega$ is produced via the four-wave mixing process, $1\omega + 1\omega \to (2-u)\omega + u\omega$ with $0 < u < 1$, by mixing two waves with different frequencies $1\omega$ and $u\omega$ in advance at the incidence.

thanks to the strong Lorentz boost, QPS provides frequency-shifted photons as the decay product of the resonance state, which become a distinct observational signal as the indication of interaction. However, as we briefly discuss in the next section, the resonance point cannot be directly captured due to the extremely narrow resonance by the weak coupling compared with the momentum uncertainty of incident photons in QPS. This situation requires an averaging process of the cross section over the possible uncertainty of the CMS energy in QPS. By this averaging, the non-negligible effect of the narrow resonance is enhanced by the square of the inverse coupling compared with the case where no resonance state is contained. If the coupling to two photons is proportional to $1/M_{\rm P}$, a huge enhancement by $M_{\rm P}^2$ is expected.

The second ingredient is the enhancement by the coherent nature of laser fields [24] or the degenerate nature of bosonic particles as illustrated in Fig. 2. This bosonic nature of the laser beam is fundamentally important, because we can induce the decay of the produced resonance state into a specific momentum space, as the principle of laser amplification itself utilizes that nature. We propose to use different frequencies between the production and inducing laser beams, respectively. As shown in the figure, the exchange of the low-mass field is interpreted as a four-wave mixing process where three waves (two of which are degenerate and one of which has a different frequency to the degenerate waves) are combined and the fourth wave emerges with a new frequency not included in the originally mixed laser waves. This four-wave mixing process is well-known in quantum optics [25]. The process is already applied to generate a different color wave from those of the incident laser beams via the nonlinear atomic processes of crystals. In other words, the proposed method is as if the atomic nonlinear process is replaced by the nonlinear process of the vacuum via the low-mass field exchange. In the context of the QED interaction, a similar approach is discussed [26] and experimental setups are proposed [27,28]. The upper limit of the photon–photon cross section is provided by this method [29]. Since each of the two photons at the first vertex annihilates into a coherent state with $1\omega$, while another photon at the second vertex is created from the coherent state with $u\omega$ with $0 < u < 1$, the interaction rate to observe the $(2-u)\omega$ frequency is eventually enhanced by a factor of $(\sqrt{N_{1\omega}}\sqrt{N_{1\omega}}\sqrt{N_{u\omega}})^2$ [17], where $N$ indicates the average number of laser photons with the individual frequencies specified by the subscripts. This cubic dependence of the interaction rate motivates us to make the laser energy per pulse as large as possible.

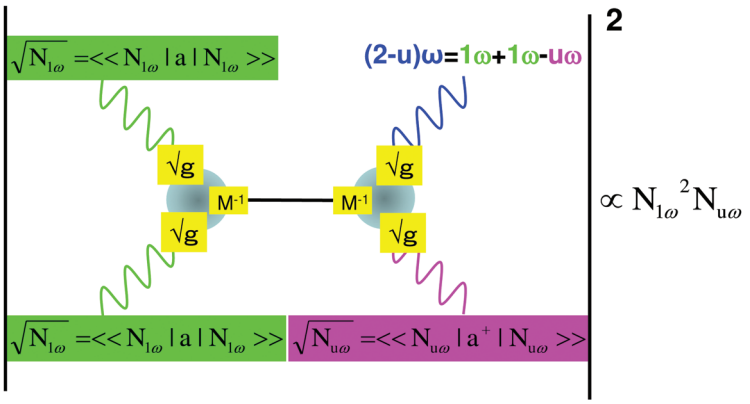


**Fig. 2.** Four-wave mixing process in the vacuum. The state $|N\rangle\rangle \equiv e^{-N/2}\sum_{n=0}^{\infty}\frac{N^{n/2}}{\sqrt{n!}}|n\rangle$, with $|n\rangle$ being the degenerate state of $n$ photons, refers to coherent states [24] with an average number of photons $N$. The coherent states are distinguished by photon frequencies specified by the individual subscripts. The probability of creating $(2-u)\omega$ with $0 < u < 1$ is expected to have cubic dependence on $N$, because the expectation values of the creation and annihilation operators associated with the individual photon legs become $\sqrt{N}$ in the scattering amplitude [17]. The effective dark field–two photon coupling $gM^{-1}$ for each vertex corresponds to the coupling in the effective interaction Lagrangian defined in Eq. (2).

In this paper, we extend the formula discussed in recent work [17,22] and then provide a prescription to relate the accessible mass-coupling domains by taking the essence of a realistic experimental constraint such as a state of the multi-frequency mode with a finite frequency bandwidth and the effect of the specification of linear polarization states, when we attempt to apply this method to experiments based on pulse lasers. The expected sensitivity to the low-mass and weakly coupling fields is provided for anticipated high-intensity laser fields available at laboratories worldwide at present and in the near future [30–32]. The result suggests that state-of-the-art technology may provide access to interactions with gravitational coupling strength and even beyond it (super-Planckian coupling) for relatively higher mass ranges in the sub-eV mass domain. We emphasize that the proposed approach is a kind of bosonic collider. Its commonality with and distinctions from a fermionic collider, e.g. LHC, is discussed as a concluding remark.

## Formulae to relate sensitivity and laser parameters

Let us briefly review the necessary parts of the extension in order to consider the effects of finite spectrum widths and the specification of the linear polarization states of the laser fields.

The effective interaction Lagrangian between two photons and an unknown low-mass scalar or pseudoscalar field $\phi$ or $\sigma$ are generalized as follows, respectively:

$$-L_\phi = gM^{-1}\frac{1}{4}F_{\mu\nu}F^{\mu\nu}\phi \quad \text{or} \quad -L_\sigma = gM^{-1}\frac{1}{4}F_{\mu\nu}\tilde{F}^{\mu\nu}\sigma, \tag{2}$$

where $M$ has a mass dimension while $g$ is a dimensionless constant. Depending on the allowed polarization combinations of two photons coupling to the dark fields, we can argue whether they are scalar-type or pseudoscalar-type in general, as we see in detail in the Appendix.

We summarize the notations and kinematics based on Eqs. (2.1)–(2.3) of Ref. [17]. We label the momenta of the four photons as illustrated in Fig. 3, where the incident angle $\vartheta$ is assumed to be

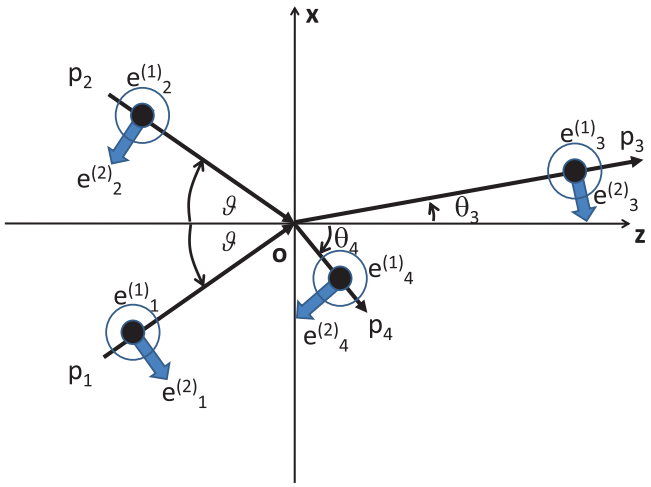


**Fig. 3.** Definitions of kinematical variables [17]. The exact definitions of the photon momenta and the polarization vectors can be found in the Appendix.

symmetric around the $z$-axis, because we assume symmetric focusing as illustrated in Fig. 1. For later convenience, we introduce an arbitrary number $u$ with $0 < u < 1$ to redefine the momenta of the final-state photons as $\omega_4 \equiv u\omega$ and $\omega_3 \equiv (2-u)\omega$. By this definition, we require $0 < \omega_4 < \omega_3 < 2\omega$. We consider the case where we measure $\omega_3$ with the specified polarization state as a signature of the interaction. With these definitions, the energy-momentum conservation in Ref. [17] is re-expressed as

$$(2-u)\omega + u\omega = 2\omega \tag{3}$$

$$(2-u)\omega\cos\theta_3 + u\omega\cos\theta_4 = 2\omega\cos\vartheta \tag{4}$$

$$(2-u)\omega\sin\theta_3 = u\omega\sin\theta_4. \tag{5}$$

From these, we also derive the following relation:

$$\frac{\sin\theta_3}{\sin\theta_4} = \frac{\sin^2\vartheta}{1 - 2\cos\vartheta\cos\theta_4 + \cos^2\vartheta}, \tag{6}$$

and

$$\omega_3 = (2-u)\omega = \frac{\omega\sin^2\vartheta}{1-\cos\vartheta\cos\theta_3}. \tag{7}$$

From Eq. (2.5) of Ref. [17], the differential cross section per solid angle of $p_3$ is expressed as

$$\frac{d\sigma}{d\Omega_3} = \left(\frac{1}{8\pi\omega}\right)^2 \sin^{-4}\vartheta \left(\frac{\omega_3}{2\omega}\right)^2 |\mathcal{M}_S|^2, \tag{8}$$

where $|\mathcal{M}_S|^2$ is the square of the invariant scattering amplitude including the resonance state in the $s$-channel with a sequence of four-photon polarization states $S = \beta_1\beta_2\beta_3\beta_4$ specified by the polarization vectors $\vec{e}_i{}^{(\beta_i)}$ with $i = 1, 2, 3, 4$ for the photon labels, whereas $\beta = 1, 2$ are a kind of the linear polarization as indicated in Fig. 3. As we discuss how to evaluate the amplitudes in

the Appendix, $S = 1111, 2222, 1122, 2211$ and $S = 1212, 1221, 2112, 2121$ give the non-vanishing invariant amplitudes for scalar and pseudoscalar exchanges, respectively.

The enhancement by the inducing laser field labeled $p_4$ is limited to the intrinsic spectrum width of the inducing laser energy due to energy-momentum conservation, which is defined as

$$\delta\omega_4 \equiv \overline{\omega_4} - \underline{\omega_4} = (\delta u)\omega, \tag{9}$$

where $\delta u \equiv \overline{u} - \underline{u}$ with $0 < \overline{u} < 1, 0 < \underline{u} < 1$, and $\overline{u} > \underline{u}$. The overlines and underlines attached to the simple variables indicate the allowed maximum and minimum values, respectively. This notation is used throughout the paper, unless confusion would occur. The spectrum width of $\omega_3$ is simultaneously constrained to

$$\delta\omega_3 \equiv \overline{\omega_3} - \underline{\omega_3} = (2 - \underline{u})\omega - (2 - \overline{u})\omega = (\delta u)\omega \tag{10}$$

due to energy-momentum conservation as well. This indicates that the energy range to detect $\omega_3$ must be consistent with $\delta\omega_4$ in order to get the full enhancement factor by the inducing laser.

By assuming that $\delta\omega_3 = \delta\omega_4$ is realized in an experimental setup, let us now calculate the cross section integrated over $\delta\omega_3$ as a function of the spectrum width parameter $(\overline{u}, \underline{u})$. Eventually, $\delta\omega_3$ gives the range of the integral via the range of scattering angle $\theta_3$. The integrated cross section over the range of $\theta_3$ from $\underline{\theta_3}$ to $\overline{\theta_3}$ is expressed as

$$\overline{\sigma} = \frac{\mathcal{F}_S \overline{|\mathcal{M}_S|^2}}{(8\pi\omega)^2 \sin^4\vartheta} \int_{\underline{\theta_3}}^{\overline{\theta_3}} \left(\frac{\omega_3}{2\omega}\right)^2 \sin\theta_3 \, d\theta_3 \equiv \frac{\mathcal{F}_S \overline{|\mathcal{M}_S|^2}}{(8\pi\omega)^2} \mathcal{I}, \tag{11}$$

by defining

$$\mathcal{I} \equiv \frac{1}{\sin^4\vartheta} \int_{\underline{\theta_3}}^{\overline{\theta_3}} \left(\frac{\omega_3}{2\omega}\right)^2 \sin\theta_3 \, d\theta_3 = \left[\frac{1}{4\cos\vartheta(1 - \cos\theta_3\cos\vartheta)}\right]_{\overline{\theta_3}}^{\underline{\theta_3}}, \tag{12}$$

where $\overline{|\mathcal{M}_S|^2}$ denotes the average $|\mathcal{M}_S|^2$ over a possible uncertainty on the incident angle $\vartheta$, as we briefly discuss below, and $\mathcal{F}_S$ corresponds to the integral over the azimuthal degree of freedom depending on the specification of photon polarizations in the initial and final states. If the scattering amplitude has axial symmetry around the $z$-axis in Fig. 3, $\mathcal{F}_S$ simply corresponds to $2\pi$. As we summarize in the Appendix, however, the axial asymmetries actually appear depending on $S$ specified by experimental conditions, which result in deviations from $2\pi$. We then convert the variable $\cos\theta_3$ to $u$ based on Eq. (7), from which we express

$$\cos\theta_3 = \frac{1}{\cos\vartheta}\left(1 - \frac{\omega}{\omega_3}\sin^2\vartheta\right) \sim 1 + \frac{1}{2}\vartheta^2\left(1 - \frac{2\omega}{\omega_3}\right) = 1 + \frac{1}{2}\vartheta^2\left(1 - \frac{2}{2-u}\right), \tag{13}$$

where terms of higher order than $\vartheta^2$ are dropped when applied to the low-mass resonance. From this, Eq. (12) is also approximated as

$$\mathcal{I} \sim \frac{\delta u}{4\vartheta^2}. \tag{14}$$

We now consider the scattering amplitudes only for the case when low-mass fields are exchanged via the resonance states in the $s$-channel. The resonance decay rate of the low-mass field with the mass $m$ into two photons is expressed as [17,22]

$$\Gamma = (16\pi)^{-1}(gM^{-1})^2 m^3. \tag{15}$$

As we calculate in detail in the Appendix, e.g. in the case of scalar field exchange, the invariant amplitude in the coplanar condition, where the plane determined by $p_1$ and $p_2$ coincides with that determined by $p_3$ and $p_4$, is expressed as

$$\mathcal{M}_S = -(gM^{-1})^2 \frac{\omega^4(\cos 2\vartheta - 1)^2}{2\omega^2(\cos 2\vartheta - 1) + m^2}, \tag{16}$$

where the denominator, denoted by $\mathcal{D}$ in the following, is the low-mass field propagator. We then introduce an imaginary part due to the resonance state by the following replacement:

$$m^2 \to (m - i\Gamma)^2 \approx m^2 - 2im\Gamma. \tag{17}$$

Substituting this into the denominator in Eq. (16) and expanding around $m$, we obtain

$$\mathcal{D} \approx -2(1 - \cos 2\vartheta)(\chi + ia), \quad \text{with} \quad \chi = \omega^2 - \omega_r^2, \tag{18}$$

where

$$\omega_r^2 = \frac{m^2/2}{1 - \cos 2\vartheta}, \quad a = \frac{m\Gamma}{1 - \cos 2\vartheta}. \tag{19}$$

From Eqs. (15) and (19), $a$ is also expressed as

$$a = \frac{\omega_r^2}{8\pi}\left(\frac{gm}{M}\right)^2, \tag{20}$$

which explicitly shows the proportionality to $M^{-2}$. We then express the squared amplitude as

$$|\mathcal{M}_S|^2 \approx (4\pi)^2 \frac{a^2}{\chi^2 + a^2}. \tag{21}$$

Theoretically, if we take the limit of $\omega \to \omega_r$, $|\mathcal{M}_S|^2 \to (4\pi)^2$ is realized from Eq. (21). This is independent of the smallness of $a \propto M^{-2}$. Meanwhile, the off-resonance case $\chi \gg a$, $|\mathcal{M}_S|^2$ equivalent to Eq. (16) is largely suppressed due to the factor $a^2 \propto M^{-4}$ for the case of a weakly coupling $M^{-1}$.

This is the most important feature arising from the resonance that overcomes the weak coupling stemming from the large relevant mass scale such as $M = M_{\rm P}$. However, we are then confronted with an extremely narrow width $a$ for, e.g., $gm \ll 1$ eV , $M \sim M_{\rm P} = 10^{27}$ eV and $\omega_r \sim 1$ eV. The solution overcoming this difficulty is an averaging process over unavoidable uncertainties of incident angles in QPS. Even if a single photon with a fixed frequency $\omega$ is focused by a lens element in QPS, the wave vector around the diffraction limit fluctuates with a wavy nature; in other words, the beam waist

$\Delta x$ at the diffraction limit and the momentum accuracy $\Delta p$ must satisfy the uncertainty principle $\Delta x \Delta p \geq \hbar/2$. Therefore, we need to distinguish between the theoretically specified momenta and the physically specified ones in QPS.

Based on Eqs. (40), (41), and (42) of Ref. [22], we express the average of the square of the invariant amplitude over a possible uncertainty on the incident angle $\vartheta$, i.e., uncertainty on the directions of the wave vectors as

$$\overline{|\mathcal{M}_S|^2} = \int_0^{\pi/2} \rho(\vartheta) |\mathcal{M}_S|^2 d\vartheta \sim \frac{(4\pi)^2}{2\omega^2} \left(\frac{\vartheta_r}{\Delta\vartheta}\right) a\pi, \tag{22}$$

where the resonance angle $\vartheta_r$ satisfies the resonance condition $\omega^2 = \omega_r = (m^2/2)/(1-\cos 2\vartheta_r)$, and we plugged the following simplest angular distribution function $\rho$[5] into Eq. (22):

$$\rho(\vartheta) = \begin{cases} 1/\Delta\vartheta & \text{for } 0 < \vartheta \leq \Delta\vartheta \\ 0 & \text{for } \Delta\vartheta < \vartheta \leq \pi/2 \end{cases}, \tag{23}$$

which is normalized to the physically possible range $0 < \vartheta \leq \pi/2$. The incident angle uncertainty $\Delta\vartheta$ can be as large as that determined from geometrical optics[6]:

$$\Delta\vartheta \sim \frac{d}{2f}, \tag{24}$$

with the common beam diameter $d$ and focal length $f$ for both the creation and inducing beams, as illustrated in Fig. 1.

By substituting Eqs. (14), (22), and (20) into Eq. (11), we express the partially integrated averaged cross section as

$$\begin{aligned} \overline{\sigma} &= \frac{\mathcal{F}_S \overline{|\mathcal{M}_S|^2}}{(8\pi\omega)^2} \mathcal{I} \sim \frac{\mathcal{F}_S}{(8\pi\omega)^2} \cdot \frac{(4\pi)^2}{2\omega^2} \left(\frac{\vartheta_r}{\Delta\vartheta}\right) \frac{\omega^2}{16\pi} \left(\frac{gm}{M}\right)^2 \pi \cdot \frac{\delta u}{4\vartheta^2} \\ &\sim \frac{\mathcal{F}_S}{512\omega^2} \frac{\delta u}{\vartheta_r \Delta\vartheta} \left(\frac{gm}{M}\right)^2 = \frac{1}{512} \left(\frac{\lambda}{2\pi}\right)^2 \frac{\delta u}{\vartheta_r \Delta\vartheta} \mathcal{F}_S \left(\frac{gm}{M}\right)^2. \end{aligned} \tag{25}$$

In the averaging process, among a possible range of $\vartheta$, only $\vartheta \sim \vartheta_r$ effectively contributes to the cross section because of the narrow width $a$ in Eq. (20) for a large $M$. The second line in Eq. (25) takes this aspect into account. For the last equation, $\omega$[eV] $= 2\pi\hbar c/\lambda$ with $\hbar = c = 1$ is substituted, where $\lambda$ is the wavelength of the creation laser field.

We now express the yield of frequency-shifted photons $\mathcal{Y}$ as a function of the spectrum width parameter $(\overline{u}, \underline{u})$:

$$\mathcal{Y} = \mathcal{L}\overline{\sigma}, \tag{26}$$

[5] This step-like distribution might be oversimplified; however, it is useful to provide a conservative sensitivity. This function must be determined eventually by the individual experimental setup based on the actual profile measurement in QPS.

[6] The Gaussian beam waist $w$ at the diffraction limit is known as $w = \frac{f\lambda}{\pi(d/2)}$ [23]. The momentum uncertainty of an incident photon at the waist is therefore $\Delta p \sim \frac{\hbar/2}{2w}$ from the uncertainty principle. With the laser photon momentum $p = \frac{h}{\lambda}$, the angle uncertainty at the waist is given by $\Delta\vartheta \sim \frac{\Delta p}{p} \sim \frac{1}{8}\frac{d/2}{f}$. This range is somewhat smaller than that of geometric optics; however, we prefer to take the classical limit as a conservative range. This is because the interaction is not necessarily limited only around the waist, but may happen at any point during the propagation into the diffraction limit, as we discuss later.

with the effective integrated luminosity $\mathcal{L}$ over propagation time of a single shot laser field with pulse duration time $\tau$, which is assumed to be common for both the creation and inducing beams. We discussed how the integrated effective luminosity should be defined in Ref. [22]. Here we briefly review the relevant part. The solution of the electromagnetic field propagation in the vacuum with a Gaussian profile in the transverse plane is well-known [23]. The transverse spatial profile of a laser field is typically Gaussian to a first order approximation in high-intensity laser systems. In this case, the electric field propagating along the $z$-direction in spatial coordinates $(x, y, z)$ is expressed as

$$E(x, y, z) \propto \frac{w_0}{w(z)} \exp\left\{-i[kz - H(z)] - r^2\left(\frac{1}{w(z)^2} + \frac{ik}{2R(z)}\right)\right\}, \tag{27}$$

where $k = 2\pi/\lambda$, $r = \sqrt{x^2 + y^2}$, $w_0$ is the minimum waist, which cannot be smaller than $\lambda$ due to the diffraction limit, and other definitions are as follows:

$$w(z)^2 = {w_0}^2\left(1 + \frac{z^2}{{z_R}^2}\right), \tag{28}$$

$$R = z\left(1 + \frac{{z_R}^2}{z^2}\right), \tag{29}$$

$$H(z) = \tan^{-1}\left(\frac{z}{z_R}\right), \tag{30}$$

$$z_R \equiv \frac{\pi {w_0}^2}{\lambda}. \tag{31}$$

The transverse beam size of the focused Gaussian laser beam is minimized at the beam waist and then expands beyond the focal point where interactions among outgoing photons are prohibited by the condition that two photons propagate into opposite directions in CMS. On the other hand, the exchange of a low-mass field may take place anywhere within the volume defined by the transverse area of the Gaussian laser times the focal length $f$ before reaching the focal point (see Fig. 1).

Given the Gaussian laser parameters above, the effective integrated luminosity $\mathcal{L}$ over the propagation volume of a laser pulse can be defined as follows [22]. At an instant, the interaction is limited within a region over $c\tau$ where the average number of photons $N_c$ and $N_i$ are available for creation and inducing processes, respectively. Luminosity at a point $z$ integrated over pulse duration $\tau$ is expressed as

$$\mathcal{L}(z) = \frac{I(N_c, N_i)}{\pi w^2(z)} = \frac{I(N_c, N_i)}{\pi w_0^2}\frac{z_R^2}{z^2 + z_R^2}, \tag{32}$$

where $I(N_c, N_i)$ denotes a dimensionless intensity depending dominantly on the average number of creation and inducing photons, $N_c$ and $N_i$, respectively, within the duration time $\tau$. The expression $w^2(z)$ in Eq. (28) is substituted. During the propagation over the focal length $f$, the effective number of interacting regions or the number of virtual bunches $b$ is expressed as $b = f/(c\tau)$. Therefore, the effective integrated luminosity $\mathcal{L}$ over pulse propagation time averaged over the focal length $f$ is finally expressed as

$$\mathcal{L} = b\int_0^f f^{-1}\mathcal{L}(z)dz = \frac{I(N_c, N_i)}{c\tau\lambda}\tan^{-1}\left(\frac{f}{z_R}\right). \tag{33}$$

In the case of charged particles or fermionic beams, the dimensionless intensity $I$ corresponds to the square of the number of particles per bunch, which is the combinatorics to take two fermions from individual colliding beam bunches. On the other hand, in the case of four-wave mixing, all photons are in quantum coherent states with the inducing nature resulting in cubic dependence, as we discussed. By taking this aspect into account, we define the dimensionless intensity included in $\mathcal{L}$ as follows:

$$I(N_c, N_i) \equiv C_{mb} N_c^2 \mathcal{A} N_i, \tag{34}$$

where $C_{mb}$ is a factor to consider combinatorics for the choice of two photons in the creation beam and one photon in the inducing beam by extending the argument for the single-frequency mode [17] to the multi-frequency mode, as discussed below, and $\mathcal{A}$ is an acceptance factor for the inducing photons to satisfy energy-momentum conservation in the final state.

The acceptance factor $\mathcal{A}$ is introduced because the process occurs only in a small portion $\delta\theta_4$ of the entire angular spectrum with the whole strength $N_i$ distributed over the total range of $\Delta\theta_4$; hence,

$$\mathcal{A} \equiv \frac{\delta\theta_4}{\Delta\theta_4} = \frac{\delta\theta_4}{\Delta\vartheta}, \tag{35}$$

which is much smaller than unity. Here $\Delta\theta_4$ is further assumed to be common with that of the creation beam $\Delta\vartheta$ by sharing the same optics as that of the creation beam. $\delta\theta_4$ is constrained by the spectrum width of $\omega_4 = u\omega$ and, therefore, is described as a function of the spectrum width parameter $(\overline{u}, \underline{u})$ as follows:

$$\delta\theta_4 = \left( \sqrt{\frac{2-\underline{u}}{\underline{u}}} - \sqrt{\frac{2-\overline{u}}{\overline{u}}} \right) \vartheta \equiv \mathcal{U}\vartheta. \tag{36}$$

This relation is obtained from energy-momentum conservation as follows. Equation (5) gives the ratio $\mathcal{R}$ defined by

$$\mathcal{R} \equiv \frac{\sin\theta_3}{\sin\theta_4} = \frac{\omega_4}{\omega_3} = \frac{u}{2-u}. \tag{37}$$

By equating Eqs. (37) and (6), we obtain

$$\cos\theta_4 = \frac{\mathcal{R}(1+\cos^2\vartheta) - \sin^2\vartheta}{2\mathcal{R}\cos\vartheta}. \tag{38}$$

Neglecting higher order terms greater than $\vartheta^2$, we approximate $\theta_4$ as

$$\theta_4 \sim \sqrt{\frac{1}{\mathcal{R}}}\vartheta = \sqrt{\frac{2-u}{u}}\vartheta. \tag{39}$$

For a low-mass case $m \sim 2\vartheta\omega$ with $\vartheta \ll 1$, $\theta_4$ is also small via $\theta_4 \sim \mathcal{R}^{-1/2}\vartheta$ from Eq. (39). Eventually the emission angle of the signal, $\theta_3$, also becomes small via $\theta_3 \sim \mathcal{R}^{1/2}\vartheta$ from Eqs. (37) and (39). This is the reason why the creation and inducing beams are all aligned into the same optical axis $z$, as illustrated in Fig. 1, by which a chance to enhance the inducing process is maximized. We note here that we have only to search for $(2-u)\omega$ as the signature of the four-wave mixing process without measuring the emission angle $\theta_3$ directly.

We then consider the effect of multi-frequency mode of a short pulse laser via the following argument on the combinatorics factor $C_{mb}$ in the mixing process. This is physically unavoidable, because a pulse laser with a short time duration must contain the corresponding energy uncertainty in principle. We assume that photons of a creation laser pulse in a state of multi-frequency mode can be uniformly divided into $n_c$ frequency bins, namely, forming a uniform frequency density within the frequency bandwidth of the creation laser pulse, each of which forms a coherent state of the individual frequency. We also assume $n_i$ for the inducing laser pulse as well. All frequencies as a result of the possible mixing between creation and inducing frequencies must be detectable by an experimental setup in order for the following argument to be valid. We also assume that all the frequency modes share a common focusing length and beam diameter independent of the wavelengths, as illustrated in Fig. 1. In this model case, the dimensionless intensity in Eq. (34) included in the luminosity definition is expected to be

$$I \propto \frac{1}{2}n_c^2\left(\sqrt{\frac{N_c}{n_c}}\sqrt{\frac{N_c}{n_c}}\right)^2 n_i\left(\sqrt{\frac{N_i}{n_i}}\right)^2 = \frac{1}{2}{N_c}^2 N_i, \tag{40}$$

where square roots are enhancement factors due to the coherent states of individual frequency bins, $\frac{1}{2}n_c^2$ corresponds to combinatorics to choose the initial two photons within the $n_c$ frequency bins of a creation laser pulse by allowing the choice of two photons even within the same frequency bin, while $n_i$ is the degree of freedom to choose one frequency bin out of $n_i$ bins. We thus find $C_{mb} = \frac{1}{2}$, which is the same dimensionless intensity as discussed in Ref. [22] after all.

The effect of the multi-frequency mode is not seen directly in terms of the combinatorics; however, we note that choosing two photons $\omega_1$ and $\omega_2$ out of $n_c$ bins implies that the incident two-photon energies could be different, which deviates from the simplest assumption of the symmetric angle of incidence with equal photon energies, as illustrated in Fig. 1. However, we can always find a reference frame by a Lorentz boost that exactly satisfies the symmetric conditions by considering the inverse process of the massive particle decay into two photons starting from the rest frame of that particle, because the interaction is enhanced only when the resonance condition $m \sim 2\vartheta\omega$ is fulfilled. Instead, $p_3$ in QPS must contain fluctuations by this boost effect. Therefore, as long as the experimental coverage on $p_3$ with respect to the additional fluctuations is broad enough, the integrated interaction rate over the detector acceptance is unchanged from the case with single mode lasers. In order to estimate the necessary coverage of $\omega_3$ approximately, we may redefine $\omega \equiv (\omega_1 + \omega_2)/2$ as the average value between two arbitrarily selected incident photon energies by taking the approximation where the transverse momentum of the produced massive particle is negligibly small compared to the longitudinal momentum of the produced particle in QPS, and all equations in Eqs. (3)–(6) are restored, because they are simply scaled by the newly defined $\omega$. Therefore, the arguments so far are approximately valid even in the case of multi-mode lasers. Suppose that the bandwidths of the creation and inducing beams are defined, respectively, as

$$\langle\omega\rangle - \Delta\omega \leq \omega \leq \langle\omega\rangle + \Delta\omega \tag{41}$$

$$\langle\omega_4\rangle - \Delta\omega_4 \leq \omega_4 \leq \langle\omega_4\rangle + \Delta\omega_4, \tag{42}$$

where $\langle\cdots\rangle$ denotes an average of each frequency distribution, while $\Delta$ indicates half of the full bandwidth of each frequency. According to the last part of Eq. (9), $\delta\omega_4$ varies depending on an

arbitrarily chosen $\omega$. However, $u$ is actually defined with respect to $\omega$. Therefore, any chosen $\omega$ are absorbed into the definition of $u \equiv \omega_4/\omega$. Thus only the first part of Eq. (9) becomes essentially relevant; it is determined by the intrinsic character of the prescribed inducing laser beam independent of the creation laser frequency $1\omega$. Accordingly, an experiment should be designed so that all the modified range of $\delta\omega_3$ via the relation Eqs. (9) and (10) is acceptable. Let us introduce new notations to describe the modified range of $\omega_3$ due to the shift of the averaged $\omega$ in order to distinguish it from $\delta\omega_3$ intrinsically caused by $\delta\omega_4$ via Eqs. (9) and (10). The modified upper and lower edges of $\omega_3$ can be defined, respectively, as

$$\overline{\omega_3'} \equiv 2\overline{\omega} - \underline{\omega_4} = 2(\langle\omega\rangle + \Delta\omega) - (\langle\omega_4\rangle - \Delta\omega_4) \equiv \langle\omega_3\rangle + \Delta\omega_3 \tag{43}$$

$$\underline{\omega_3'} \equiv 2\underline{\omega} - \overline{\omega_4} = 2(\langle\omega\rangle - \Delta\omega) - (\langle\omega_4\rangle + \Delta\omega_4) \equiv \langle\omega_3\rangle - \Delta\omega_3, \tag{44}$$

with $\langle\omega_3\rangle \equiv 2\langle\omega\rangle - \langle\omega_4\rangle$ and $\Delta\omega_3 \equiv 2\Delta\omega + \Delta\omega_4$. As long as an experiment can accept $\omega_3$ in the range $\underline{\omega_3'} \le \omega_3 \le \overline{\omega_3'}$, the expected yield in the following paragraphs is valid. Naturally, the range of $\delta\omega_3$ via the intrinsic $\delta\omega_4$ is fully contained in this modified range. In the case of the multi-frequency mode, strictly speaking, $u$ should be defined as $u \equiv \langle\omega_4\rangle/\langle\omega\rangle$, resulting in $\overline{u} \equiv (\langle\omega_4\rangle + \Delta\omega_4)/\langle\omega\rangle$ and $\underline{u} \equiv (\langle\omega_4\rangle - \Delta\omega_4)/\langle\omega\rangle$. For all of the arguments in this paper, $u$ and $\delta u$ are implicitly assumed to be defined based on the average frequencies.

We now express the yield $\mathcal{Y}$ by substituting Eqs. (34), (35), and (25) into Eq. (26):

$$\mathcal{Y} \equiv K_0(\lambda, \tau) K_1(f, d) K_2(\overline{u}, \underline{u}) \mathcal{F}_S \left(\frac{gm}{M}\right)^2 C_{mb} {N_c}^2 N_i, \tag{45}$$

where

$$K_0(\lambda, \tau) \equiv \frac{\lambda}{c\tau} \tag{46}$$

indicates that a shorter pulse duration time $c\tau \to \lambda$ has the maximum gain on the yield,

$$K_1(f, d) \equiv \frac{1}{2048\pi^2(\Delta\vartheta)^2} \tan^{-1}\left(\frac{f}{z_R}\right) \sim \frac{1}{512\pi^2}\left(\frac{f}{d}\right)^2 \tan^{-1}\left(\frac{\pi d^2}{4f\lambda}\right) \tag{47}$$

with $w_0 = f\lambda/(\pi(d/2))$ for $z_R = \pi w_0^2/\lambda$ [23] being the parameter relevant to optics alone, and where

$$K_2(\overline{u}, \underline{u}) \equiv \mathcal{U}\delta u = \left(\sqrt{\frac{2-\underline{u}}{\underline{u}}} - \sqrt{\frac{2-\overline{u}}{\overline{u}}}\right)(\overline{u} - \underline{u}) \tag{48}$$

is the laser spectrum width parameter determined from the spectrum width of the inducing laser field, $\delta\omega_4$.

From Eq. (45) we finally obtain the expression for the coupling parameter $g/M$ to discuss the sensitivity as a function of $m$ for a given experimental parameter via the following equation:

$$\frac{g}{M} = m^{-1}\sqrt{\frac{\mathcal{Y}}{K_0 K_1 K_2 \mathcal{F}_S C_{mb} {N_c}^2 N_i}}. \tag{49}$$

For convenience in designing experiments, we also consider the case where duration times are not equal between the creation beam $\tau_c$ and the inducing beam $\tau_i$. Since the yield is increased by the quadratic dependence on the creation beam intensity, it is natural to realize the case $\tau = \tau_c \leq \tau_i$ in experiments. If this is the case, the accessible coupling is re-expressed as

$$\frac{g}{M} = m^{-1}\sqrt{\frac{\mathcal{Y}}{K_0 K_1 K_2 \mathcal{F}_{\mathcal{S}} C_{mb} {N_c}^2 N_i (\tau_c/\tau_i)}}. \tag{50}$$

## Expected sensitivity

First we summarize the key control parameters or experimentally adjustable knobs based on the arguments in the previous sections. The resonance condition is satisfied if $m \sim 2\vartheta\omega$. However, instead of hitting the resonance point directly, our approach is to take the average of the squared scattering amplitude over the possible incident angle uncertainty $\Delta\vartheta$ in QPS by the focused laser beams. Changing the focal length introduces different $\Delta\vartheta$, i.e., a different range of the angular integral for the averaging. If a resonance peak is contained in that range, the resonance effect appears as the integrated result. The basic strategy of this proposal is therefore to change the focal length, attempting to search for the appearance of four-wave mixing photons, which approximately gives a mass range via the relation $m \leq 2\omega\Delta\vartheta$. Thus, this knob provides variations along the mass axis, $m$. On the other hand, the four-wave mixing yield is enhanced by the cubic product of the laser intensities. Therefore, changing the laser intensities gives large variations along the coupling axis, $g/M$. If a significant signature is found, we can localize the domain in the $(m, g/M)$ plane by adjusting these two knobs.

In addition, there are knobs on the polarization states of laser fields. As we discuss in detail in the Appendix, depending on the types of exchanged fields, different polarization correlations are expected between the two photons in the initial and final states. In the case of the scalar field exchange, which is the first of Eq. (2), the possible linear polarization states in the four-wave mixing process are expressed as follows:

$$\begin{aligned}
\omega\{1\} + \omega\{1\} &\to (2-u)\omega\{1\} + u\omega\{1\} \\
\omega\{1\} + \omega\{1\} &\to (2-u)\omega\{2\} + u\omega\{2\},
\end{aligned} \tag{51}$$

where photon energies from the initial to final states are denoted with the linear polarization states $\{1\}$ and $\{2\}$, which are orthogonal to each other. On the other hand, in the case of the pseudoscalar field exchange with the second of Eq. (2), the possible linear polarization states are expressed as:

$$\begin{aligned}
\omega\{1\} + \omega\{2\} &\to (2-u)\omega\{2\} + u\omega\{1\} \\
\omega\{1\} + \omega\{2\} &\to (2-u)\omega\{1\} + u\omega\{2\}.
\end{aligned} \tag{52}$$

By choosing physically allowed combinations of the linear polarizations, we can distinguish the types of exchanged fields, while we can estimate the background processes by requiring false combinations on purpose.

Let us now briefly review some of the major high-intensity laser facilities in the world, including ongoing projects, which can provide more than 100 J per pulse. There are typically two classes of laser systems to achieve high intensity: a moderate pulse energy per tens of fs short duration and a large pulse energy per several ns duration. The established choices of the laser technology for

the former and latter classes are Ti:sapphire-based lasers and Nd:glass-based lasers typically dedicated to laser fusion studies, respectively. We note that energy per shot is more important than pulse duration for the proposed method, because the interaction rate is cubic to the numbers of photons, while it is inversely proportional to pulse duration. On the other hand, the typical repetition rates for such high-energy pulse lasers are currently limited to at most every minute and a few shots per day for the former and latter classes, respectively. The frontiers of the former class are *VULCAN 10PW* 300 J/30 fs [51], *APOLLON* 150 J/15 fs [52], and what is prepared for the Extreme Light Infrastructure (ELI) project by combining 20 APOLLON-type lasers [53]. Examples of the latter class are *GEKIKO-XII* 0.1–1 kJ combining 12 beam lines [54], *VULCAN* 2.6 kJ combining 8 beam lines [55], *FELIX* 10 kJ combining 4 beam lines [54], *OMEGA* 30 kJ combining 60 beam lines [56], *PETAL with quad LMJ* 1.5–80 kJ [57], *LMJ* 1.8 MJ combining 240 beam lines [58], and *NIF* 1.8 MJ combining 192 beam lines [59]. The quoted numbers above should be regarded as rough references that can change depending on the operational conditions and the progress of the ongoing projects. The bottleneck of the currently available laser systems with respect to the proposed method, *the higher the pulse energy, the lower the repetition rate*, is going to be improved. The proposed coherent amplification network (CAN) technique [60] adopts the coherent addition of highly efficient fiber lasers, which is, in principle, operational at a higher repetition rate, resolving the heat problem typically seen in Nd:glass-based lasers. An international project, the International Coherent Amplification Network (ICAN), has been launched [61]. This is also encouraging for the high-energy physics community aiming at a much higher energy than the conventional acceleration technique, because a high average power is eventually necessary for high-luminosity physics, even based on the new acceleration scheme, laser wakefield acceleration (LWFA) [62]. High-intensity lasers can serve as an extension to the traditional high-energy physics course as well as the novel type of physics as discussed in this paper. The International Center for Zetta- and Exawatt Science and Technology (IZEST) has been launched toward the integration of high-energy physics and high-field science [64]. These combined efforts are reviewed in our recent article [63].

Figure 4 indicates explorable domains in the $(m, g/M)$ plane by searching for the four-wave mixing process by counting the number of photons in the frequency band $\omega_3' \le \omega_3 \le \overline{\omega_3'}$, where $\mathcal{F}_S = 2\pi$ is used because any $\mathcal{F}_S$ are on the same order as those in the axial symmetric case, as we discuss in detail in the Appendix, and the intention of this plot is not the separation between scalar and pseudoscalar fields. With the help of the advanced technology, frequency-band selection around the optical frequency domain can be achieved by combining a set of high-quality optical elements such as prisms, dichroic mirrors, and filters to shut out the non-interacting $1\omega$ and $u\omega$ laser fields at the downstream of Fig. 1 before the detection of $\omega_3$ with the sensitivity to a single photon. Single-photon detection is not a difficult issue as it is given by any conventional photomultiplier with a typical gain factor of $\sim 10^6$, with respect to the single photoelectron caused by the incidence of the single photon, especially in an environment where coincidence signals synchronized with injections of short laser pulses in time are available for the rejection of the photodevice's dark current noise.

The brown, blue, and red lines indicate the achievable upper limits with 95% confidence level when no photon in the frequency band $\omega_3' \le \omega_3 \le \overline{\omega_3'}$ is observed per single shot focusing (see Table 33.3 in Ref. [50]), the parameters of which are summarized in Table 1. We choose the laser parameters, which depend heavily on the actual system, to be as general as possible by considering the anticipated pulse energies in the existing facilities reviewed above, where the wavelengths of production and inducing laser beams are assumed to be around 1 $\mu$m, and the focusing parameters and pulse duration time are chosen so that the laser intensity (W/cm$^2$) at the surface of the final focusing device is lower than the

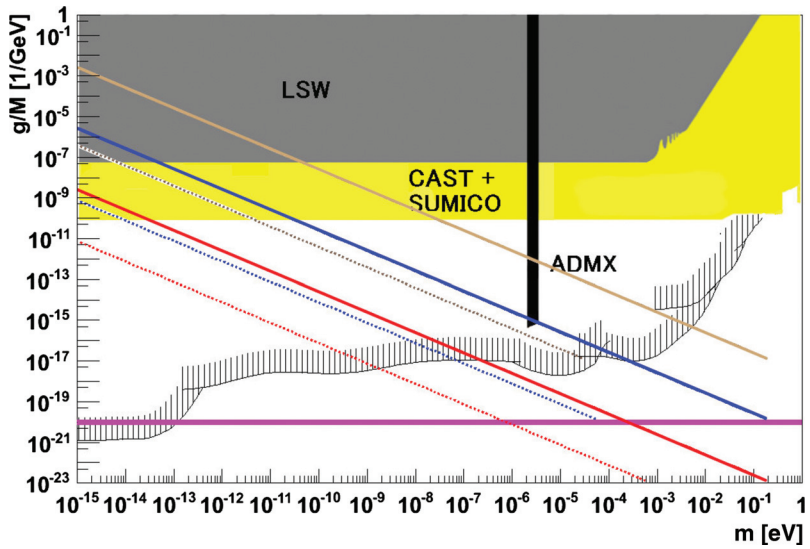


**Fig. 4.** Upper limits of the sensitivities in the $(m, g/M)$ plane by searching for the four-wave mixing process with a single laser shot. The brown, blue, and red lines indicate the achievable upper limits with 95% confidence level, assuming that no background process is included, when no photon with frequency upshift is observed per single shot focusing, the laser parameters of which are summarized in Table 1 based on the formula Eq .(24) with $C_{mb} = 1/2$. Here $\mathcal{F}_s = 2\pi$ is used because any $\mathcal{F}_S$ are on the same order as those in the axial symmetric case and the intention of this plot is not the separation between scalar and pseudoscalar fields. The solid and dashed lines are the cases with short and long focal lengths. The excluded gray, black, and yellow domains via dark field–photon coupling are quoted from Ref. [19]. The upper limits from the searches for the non-Newtonian force, obtained by reinterpreting them based on the effective Yukawa interaction between test bodies [34], are also shown with black shaded curves. The limit of the gravitational coupling strength is added by assuming $g \sim \mathcal{O}(\alpha_{\rm qed}) \sim 10^{-2}$ and $M = M_{\rm P} \sim 10^{18}$ GeV as an order estimate based on the model [5].

**Table 1.** Laser parameters to estimate the sensitivity to mass-coupling domains by searching for the four-wave mixing process in the vacuum.

| Laser parameters | Brown lines | Blue lines | Red lines |
|---|---|---|---|
| Production energy | 200 J | 20 kJ | 2 MJ |
| Inducing energy | 200 J | 20 kJ | 2 MJ |
| Inducing spectrum width $\delta u$ | 0.1 | 0.1 | 0.1 |
| Pulse duration time $\tau (= \tau_c = \tau_i)$ | 1 ns | 1 ns | 1 ns |
| Diameter at the final focusing mirror $d$ | 40 cm | 80 cm | 800 cm |
| Intensity at the final focusing mirror | $3.2 \times 10^8$ W/cm$^2$ | $8.0 \times 10^9$ W/cm$^2$ | $8.0 \times 10^9$ W/cm$^2$ |
| Fluence at the final focusing mirror | 0.32 J/cm$^2$ | 8.0 J/cm$^2$ | 8.0 J/cm$^2$ |
| Short focal length $f$ (mass range) | 1.5 m ($< 0.22$ eV) | 3 m ($< 0.22$ eV) | 30 m ($< 0.22$ eV) |
| $gm/M$ at 95% C.L. for short focal length | $2.52 \times 10^{-27}$ | $2.52 \times 10^{-30}$ | $2.52 \times 10^{-33}$ |
| Long focal length $f$ (mass range) | 10 km ($< 32\,\mu$eV) | 10 km ($< 65\,\mu$eV) | 10 km ($< 0.65$ meV) |
| $gm/M$ at 95% C.L. for long focal length | $3.88 \times 10^{-31}$ | $7.61 \times 10^{-34}$ | $7.56 \times 10^{-36}$ |

damage threshold—typically $10^{13}$ W/cm$^2$—by more than three orders of magnitude, considering the future pulse compression option with sub-ps duration. In addition, the fluence (J/cm$^2$) is also required to be lower than the typical damage threshold, 10 J/cm$^2$, for ns duration. The solid and dashed lines are for the short and long focal lengths, respectively. This figure provides a baseline from which to argue the single shot sensitivities. Increasing the shot statistics and shortening pulse duration time improves the sensitivity. These depend on the future development of high-intensity laser technology.

We note that the physical background process from the QED box diagram is totally negligible, as discussed in Ref. [17], essentially due to the smallness of the CMS energies in QPS. The generation of high harmonics from residual atoms is expected to be a background process by the atomic recombination process between the ejected electrons and the parent ion after tunneling or barrier-suppression ionization by a strong external laser field. The appearance intensity values are expected to be $1.5 \times 10^{16}\,\mathrm{W/cm^2}$ and $4.0 \times 10^{16}\,\mathrm{W/cm^2}$ for $N^{5+}$ and $O^{6+}$, respectively [33]. The vacuum pressure around the focal spot, therefore, should be kept as low as possible. The commercially available vacuum pump can achieve $\sim 10^{-10}\,\mathrm{Pa}$, where the expected number of atoms per $(100\,\mu\mathrm{m})^3$ volume can be below unity. We can estimate such a background process by requiring false combinations of linear polarization states of the initial and final photons in actual measurements. However, for simplicity, we assumed no background process in order to provide ideal sensitivity curves at this stage.

Filled areas are domains excluded by other types of laboratory experiments, focusing on axion-like particle (ALP)–photon coupling [19] as well as the upper limits from the searches for non-Newtonian forces, by reinterpreting them based on the effective Yukawa interaction between test bodies [34]. State-of-the-art methods to search for ALP at terrestrial laboratories by utilizing two-photon–axion coupling are represented by LSW (light shining through walls) [35–41], the solar axion searches CAST (CERN axion solar telescope) [45–47] and SUMICO (Tokyo axion helioscope) [42–44], and ADMX (axion dark matter experiment) [48,49]. In LSW a laser pulse together with a static magnetic field produces ALP; the ALP penetrates an opaque wall thanks to its weakly coupling nature with matter, and it then regenerates a photon via coupling to the same static magnetic field located over the wall. The solar axion search is similar to LSW, but different in terms of the production part. In the Sun, two incoherent photons may produce ALP. The long-lived ALP penetrates the Sun and the atmosphere in the earth, and they regenerate photons by coupling to a prepared static magnetic field on the earth. ADMX utilizes a microwave cavity immersed in a static magnetic field, and ALP passing through the cavity can be resonantly converted into real microwave photons.

Bosonic enhancement is partly utilized in these axion searches, where the axion decay is commonly induced under static magnetic field. However, the static magnetic field is not in a degenerate state with a narrow momentum range. Therefore, the enhancement of the decay is limited. The enhancement of the production rate is also limited because of the broad CMS energy range when choosing two photons for the production of the resonance state. We emphasize that the most unusual aspect of our approach is in the field theoretical treatment, by which we can incorporate the nature of the resonance production and decay under degenerate fields. This is in contrast to the classical treatment prescribed for past axion searches. Moreover, the bulk static magnetic field has a limitation of increasing the field strength compared with the recent leap in laser energy [30–32], where cutting-edge laser technology is about to exceed Avogadro's number of photons per laser pulse ($200\,\mathrm{kJ} \sim 10^{23}$ optical photons).

## Conclusion

We have shown that the sensitivity to dark fields by searching for the four-wave mixing process of laser fields is expected to be able to reach the sub-eV mass range with a coupling strength as weak as that of gravity and even beyond it, if cutting-edge laser technology is properly combined. Even before reaching extremely high fields, we have many opportunities to test the light cold dark matter candidate with the proposed method. This high sensitivity is essentially realized by the bosonic nature of laser fields.

As a concluding remark, we emphasize some of features to search for the four-wave mixing process by comparing them with those in high-energy colliders as follows. As an example, let us remind ourselves of the Higgs production at LHC as a search for the heavy scalar field.

First, resonance searches in collider experiments are based on measurement of the invariant mass distribution of a produced resonance state. In searching for a resonance state in QPS, in contrast, we have the unavoidable CMS energy uncertainty originating from the uncertainty principle of optical waves compared with the extremely narrow resonance width due to the weak coupling. We are unable to reconstruct the invariant mass distribution directly, though the interaction probability is still affected by the integrated effect over the possible CMS energy uncertainty. By observing the appearance or disappearance of the four-wave mixing signal, however, one can determine the order of the mass scale from the incident wavelength and the collision geometry, a significant difference from a conventional collider's approach.

Second, in the case of Higgs at LHC, the dominant production channel is the gluon–gluon fusion process and the produced Higgs resonance state decays into two photons, where neither the initial gluons nor the final photons are in degenerate states. Therefore, all fields should be treated incoherently, and the decay process occurs only via spontaneous processes in the vacuum, i.e., two photons in the final state are created from the pure vacuum state $|0\rangle$. On the other hand, in the case of photon–photon interactions under laser fields, all photons are annihilated into and created from the degenerate states. This situation results in an interaction rate with cubic dependence on the average number of photons included in the laser fields, which is in contrast to the square dependence of the number of charged particles in the luminosity of fermionic particle colliders. The prime mission of the energy frontier of high-energy physics is, of course, to produce new heavy particles; therefore, the realization of the high CMS energy is the most important task, while the sensitivity to weakly coupling fields is sacrificed. The dimensionless intensity included in luminosity is proportional to the square of the number of charged particles per bunch, which is typically $\sim 10^{11}$ particles due to the physical limitations of the space-charge effect. Even if we could collide them at a maximum of 1 GHz over a three-year data taking period, the integrated dimensionless intensity reaches $(10^{11})^2 \cdot 10^9 \cdot 10^8 = 10^{39}$. This indicates that it is practically impossible to reach the sensitivity to cross sections with coupling including $M_{\mathrm{P}}^{-1}$. In contrast, with the proposed method, we can expect a dimensionless intensity of $(10^{23})^3 = 10^{69}$ even with a single laser shot including Avogadro's number of photons. This manifestly shows how the proposed approach can be sensitive to weakly coupling interactions.

Therefore, in addition to the present most powerful experimental approach, such as heavy boson searches at the high-energy fermionic collider, the proposed coherent bosonic collider with the inducing mechanism— simply speaking, four-wave mixing by focused high-intensity laser fields—opens up a novel opportunity to bridge particle physics and cosmology in the so-far-unprobed low-mass and weakly coupling domains under controllable laboratory environments.

## Acknowledgments

K. Homma expresses his deep gratitude to T. Tajima and G. Mourou for many aspects relevant to this subject. He has greatly benefited from the valuable suggestions and support of D. Habs, K. Witte, S. Sakabe, and V. Zamfir. He cordially thanks Y. Fujii for the long-term discussions on the theoretical aspects. This work was supported by the Grant-in-Aid for Scientific Research No. 24654069 from MEXT of Japan.

## Appendix: Polarization dependence of scattering amplitudes and axial asymmetric factors $\mathcal{F}_S$

Given the scattering configuration illustrated in Fig. 3, the Lorentz invariant $s$-channel scattering amplitudes defined in Eq. (2) have the following basic form:

$$\mathcal{M}_S = -(gM^{-1})^2 \frac{\mathcal{V}_{ab}^{[1]}\mathcal{V}_{cd}^{[2]}}{(p_1+p_2)^2+m^2}, \tag{A1}$$

where $S \equiv abcd$ with $a, b, c, d = 1$ or 2, respectively, denotes a sequence of four-photon polarization states and $m$ is the mass of the scalar or pseudoscalar field.

The vertex factors in the numerator for the case of the scalar field exchange ($SC$) are defined as

$$\begin{aligned}
\mathcal{V}_{ab}^{[1]SC} &\equiv \left\langle p_2, e_2^{(b)} \left| \frac{1}{4} F_{\mu\nu}F^{\mu\nu} \right| p_1, e_1^{(a)} \right\rangle = \frac{1}{2}\langle p_2, e_2^{(b)}|F_{\mu\nu}|0\rangle\langle 0|F^{\mu\nu}|p_1, e_1^{(a)}\rangle \\
\mathcal{V}_{cd}^{[2]SC} &\equiv \left\langle p_4, e_4^{(d)} \left| \frac{1}{4} F_{\mu\nu}F^{\mu\nu} \right| p_3, e_3^{(c)} \right\rangle = \frac{1}{2}\langle p_4, e_4^{(d)}|F_{\mu\nu}|0><0|F^{\mu\nu}|p_3, e_3^{(c)}\rangle,
\end{aligned} \tag{A2}$$

while those for the case of the pseudoscalar exchange ($PS$) are given by

$$\begin{aligned}
\mathcal{V}_{ab}^{[1]PS} &\equiv \left\langle p_2, e_2^{(b)} \left| \frac{1}{4} F_{\mu\nu}\epsilon^{\mu\nu\rho\sigma}F_{\rho\sigma} \right| p_1, e_1^{(a)} \right\rangle = \frac{1}{2}\langle p_2, e_2^{(b)}|F_{\mu\nu}|0\rangle\langle 0|\epsilon^{\mu\nu\rho\sigma}F_{\rho\sigma}|p_1, e_1^{(a)}\rangle \\
\mathcal{V}_{cd}^{[1]PS} &\equiv \left\langle p_4, e_4^{(d)} \left| \frac{1}{4} F_{\mu\nu}\epsilon^{\mu\nu\rho\sigma}F_{\rho\sigma} \right| p_3, e_3^{(c)} \right\rangle = \frac{1}{2} < p_4, e_4^{(d)}|F_{\mu\nu}|0\rangle\langle 0|\epsilon^{\mu\nu\rho\sigma}F_{\rho\sigma}|p_3, e_3^{(c)}\rangle.
\end{aligned} \tag{A3}$$

Let us define the polarization vectors and momentum vectors for the four photons in Fig. 3 as follows:

$$e_i^{(1)} = (0, 1, 0), \tag{A4}$$

$$\begin{aligned}
e_1^{(2)} &= (-\cos\vartheta, 0, \sin\vartheta), \quad e_2^{(2)} = (-\cos\vartheta, 0, -\sin\vartheta), \\
e_3^{(2)} &= (-\cos\theta_3, 0, \sin\theta_3), \quad e_4^{(2)} = (-\cos\theta_4, 0, -\sin\theta_4), \\
p_1 &= (\omega\sin\vartheta, 0, \omega\cos\vartheta; \omega), \quad p_2 = (-\omega\sin\vartheta, 0, \omega\cos\vartheta; \omega), \\
p_3 &= (\omega_3\sin\theta_3, 0, \omega_3\cos\theta_3; \omega_3), \quad p_4 = (-\omega_4\sin\theta_4, 0, \omega_4\cos\theta_4; \omega_4).
\end{aligned} \tag{A5}$$

Based on these vectors, let us summarize the basic relations between momenta and polarization vectors with photon labels $i = 1, 2, 3, 4$ as follows:

$$\left(p_i e_j^{(1)}\right) = 0 \tag{A6}$$

for the coplanar condition, where the plane determined by $p_1$ and $p_2$ is the same as that of $p_3$ and $p_4$,

$$\left(e_i^{(1)} e_j^{(1)}\right) = 1, \quad \text{and} \quad \left(e_i^{(1)} e_j^{(2)}\right) = 0 \tag{A7}$$

for any pair $i$, $j$, and

$$\begin{aligned}
&\left(e_i^{(2)} e_j^{(2)}\right) = 1 \quad \text{for} \quad i = j, \\
&\left(e_1^{(2)} e_2^{(2)}\right) = \cos 2\vartheta, \left(e_3^{(2)} e_4^{(2)}\right) = \cos(\theta_3 + \theta_4) \equiv \cos\theta_+, \\
&\left(e_1^{(2)} e_3^{(2)}\right) = \cos(\vartheta - \theta_3), \left(e_2^{(2)} e_4^{(2)}\right) = \cos(\vartheta - \theta_4), \\
&\left(e_1^{(2)} e_4^{(2)}\right) = \cos(\vartheta + \theta_4), \left(e_2^{(2)} e_3^{(2)}\right) = \cos(\vartheta + \theta_3).
\end{aligned} \tag{A8}$$

We then introduce a clockwise rotation of the $p_3$–$p_4$ plane from the $p_1$–$p_2$ plane defined on the $x$–$z$ plane by the azimuthal angle $\varphi$ varying from 0 to $2\pi$ around the $z$-axis in order to discuss the axial symmetry of the scattering process, when polarization vectors are fixed in an experiment. The rotated vectors are defined as

$$\begin{aligned}
p_3(\varphi) &= (\omega_3 \sin\theta_3 \cos\varphi, -\omega_3 \sin\theta_3 \sin\varphi, \omega_3 \cos\theta_3; \omega_3) \\
p_4(\varphi) &= (-\omega_4 \sin\theta_4 \cos\varphi, \omega_4 \sin\theta_4 \sin\varphi, \omega_4 \cos\theta_4; \omega_4),
\end{aligned} \tag{A9}$$

and these result in

$$(p_3(\varphi) p_4(\varphi)) = \omega_3\omega_4(\cos\theta_+ - 1) = \omega^2(\cos 2\vartheta - 1), \tag{A10}$$

where the last equation is obtained from $(p_1 + p_2)^2 = (p_3 + p_4)^2$.

With the vectors defined above, the vertex factors for the scalar case are expressed as

$$\begin{aligned}
\mathcal{V}_{ab}^{[1]SC} &= (p_1 p_2)(e_1^{(a)} e_2^{(b)}) - (p_1 e_2^{(a)})(p_2 e_1^{(b)}), \\
\mathcal{V}_{cd}^{[2]SC} &= (p_3(\varphi) p_4(\varphi))(e_3^{(c)} e_4^{(d)}) - (p_3(\varphi) e_4^{(c)})(p_4(\varphi) e_3^{(d)}),
\end{aligned} \tag{A11}$$

and those for the pseudoscalar case are expressed as

$$\begin{aligned}
\mathcal{V}_{ab}^{[1]PS} &= -\epsilon^{\mu\nu\rho\sigma} p_{1\mu} p_{2\rho} e_{1\nu}^{(a)} e_{2\sigma}^{(b)} \\
V_{cd}^{[2]PS} &= -\epsilon^{\mu\nu\rho\sigma} p_3(\varphi)_\mu p_4(\varphi)_\rho e_{3\nu}^{(c)} e_{4\sigma}^{(d)}.
\end{aligned} \tag{A12}$$

We are now ready to estimate the factor $\mathcal{F}_S$ included in the partially integrated cross section in Eq. (11). First, we estimate $S = 1122$ for the scalar exchange. From the first of Eq. (A11), we obtain

$$\mathcal{V}_{11}^{[1]SC} = \omega^2(\cos 2\vartheta - 1) \equiv \mathcal{K}\omega^2. \tag{A13}$$

With

$$\begin{aligned}
\left(p_3(\varphi) e_4^{(2)}\right) &= -\omega_3(\sin\theta_3 \cos\theta_4 \cos\varphi + \cos\theta_3 \cos\theta_4) \\
\left(p_4(\varphi) e_3^{(2)}\right) &= \omega_4(\sin\theta_4 \cos\theta_3 \cos\varphi + \cos\theta_4 \cos\theta_3),
\end{aligned} \tag{A14}$$

we get

$$\left(p_3(\varphi)e_4^{(2)}\right)\left(p_4(\varphi)e_3^{(2)}\right) = -\omega_3\omega_4\{(1+\cos^2\varphi)\sin\theta_3\sin\theta_4\cos\theta_3\cos\theta_4 + (\sin^2\theta_3\cos^2\theta_4+\sin^2\theta_4\cos^2\theta_3)\cos\varphi\}, \tag{A15}$$

and then the second vertex factor in the second of Eq. (A11) is expressed as

$$\mathcal{V}_{22}^{[2]SC} = \omega_3\omega_4\{\cos\theta_+(\cos\theta_+-1)+(1+\cos^2\varphi)\sin\theta_3\sin\theta_4\cos\theta_3\cos\theta_4 + (\sin^2\theta_3\cos^2\theta_4+\sin^2\theta_4\cos^2\theta_3)\cos\varphi\}. \tag{A16}$$

For $\varphi = 0$, this coincides with $|\mathcal{V}_{11}^{[1]SC}|$ via the relation

$$\begin{aligned}\mathcal{V}_{22}^{[2]SC}(\varphi=0) &= \omega_3\omega_4\{\cos\theta_+(\cos\theta_+-1)+\sin^2\theta_+\}\\ &= \omega_3\omega_4(1-\cos\theta_+) = \omega^2(1-\cos 2\vartheta) = -\mathcal{K}\omega^2.\end{aligned} \tag{A17}$$

For a small $\vartheta$ we take the following approximations: $\sin\theta_3 \sim \sqrt{\mathcal{R}}\vartheta$ and $\sin\theta_4 \sim 1/\sqrt{\mathcal{R}}\vartheta$ from Eqs. (37) and (39), and this results in $\cos\theta_+$ as

$$\cos\theta_+ \sim 1-\vartheta^2(1+\hat{\mathcal{R}}), \tag{A18}$$

with

$$\hat{\mathcal{R}} \equiv \frac{1}{2}(\mathcal{R}+\mathcal{R}^{-1}). \tag{A19}$$

We then approximate Eq. (A16) as

$$\mathcal{V}_{22}^{[2]SC} \sim \omega_3\omega_4\vartheta^2\{\cos^2\varphi+(2\cos\varphi-1)\hat{\mathcal{R}}\} \equiv \omega_3\omega_4\vartheta^2 F(\varphi). \tag{A20}$$

This is consistent with the approximation of Eq. (A17) for a small $\vartheta$:

$$\mathcal{V}_{22}^{[2]SC}(\varphi=0) \sim \omega_3\omega_4\vartheta^2(1+\hat{\mathcal{R}}). \tag{A21}$$

By taking the square of the factorized second vertex factor, we then naturally define the factor $\mathcal{F}_S$ for the scalar case

$$\mathcal{F}_{1122}^{SC} \equiv \int_0^{2\pi} F^2(\varphi)d\varphi \sim 2\pi\left(\frac{3}{8}+3\hat{\mathcal{R}}^2-\hat{\mathcal{R}}\right). \tag{A22}$$

Second, let us estimate $S = 1212$ for the pseudoscalar field exchange as follows. From the first of Eq. (A12) with the vector definitions above, we obtain the first vertex factor as

$$\begin{aligned}
\mathcal{V}_{12}^{[1]PS} &= -p_{1\mu}p_{2\rho}\epsilon^{\mu y\rho\sigma}e_{2\sigma}^{(2)} = -p_{1\mu}p_{2\rho}\left[\epsilon^{\mu y\rho x}(-\cos\vartheta) + \epsilon^{\mu y\rho z}(-\sin\vartheta)\right] \\
&= p_{2\rho}\left[\left(p_{10}\epsilon^{0y\rho x} + p_{1z}\epsilon^{zy\rho x}\right)\cos\vartheta + \left(p_{10}\epsilon^{0y\rho z} + p_{1x}\epsilon^{xy\rho z}\right)\sin\vartheta\right] \\
&= p_{2\rho}\left[\left(-\omega\epsilon^{0y\rho x} + \omega\cos\vartheta\,\epsilon^{zy\rho x}\right)\cos\vartheta + \left(-\omega\epsilon^{0y\rho z} + \omega\sin\vartheta\,\epsilon^{xy\rho z}\right)\sin\vartheta\right] \\
&= \left[\left(-\omega\epsilon^{0yzx}p_{2z} + \omega\cos\vartheta\,\epsilon^{zy0x}p_{20}\right)\cos\vartheta + \left(-\omega\epsilon^{0yxz}p_{2x} + \omega\sin\vartheta\,\epsilon^{xy0z}p_{2z}\right)\sin\vartheta\right] \\
&= \omega^2\left[(-\cos\vartheta + \cos\vartheta)\cos\vartheta + (-\sin\vartheta - \sin\vartheta)\sin\vartheta\right] = -2\omega^2\sin^2\vartheta. \qquad \text{(A23)}
\end{aligned}$$

We also get the second vertex factor from the second of Eq. (A12), with the vector definitions above, as follows:

$$\begin{aligned}
\mathcal{V}_{12}^{[2]PS} &= -\epsilon^{\mu\nu\rho\sigma}p_{3\mu}p_{4\rho}e_{3\nu}^{(1)}e_{4\sigma}^{(2)} = -\epsilon^{\mu y\rho\sigma}p_{3\mu}p_{4\rho}e_{4\sigma}^{(2)} \\
&= -\left(-\epsilon^{\mu y\rho x}\cos\theta_4 - \epsilon^{\mu y\rho z}\sin\theta_4\right)p_{3\mu}p_{4\rho} \\
&= \left[\left(\epsilon^{0y\rho x}\cos\theta_4 + \epsilon^{0y\rho z}\sin\theta_4\right)p_{30} + \left(\epsilon^{zy\rho x}\cos\theta_4 p_{3z} + \epsilon^{xy\rho z}\sin\theta_4 p_{3x}\right)\right]p_{4\rho} \\
&= -\omega_3\left(\epsilon^{yzx}p_{4z}\cos\theta_4 + \epsilon^{yxz}p_{4x}\sin\theta_4\right) + 4\left(\epsilon^{zy0x}\cos\theta_4 p_{3z} + \epsilon^{xy0z}p_{3x}\right)p_{40} \\
&= -\omega_3\omega_4\left[\left(\cos^2\theta_4 + \sin^2\theta_4\cos\varphi\right) + (-\cos\theta_4\cos\theta_3 + \sin\theta_4\sin\theta_3\cos\varphi)\right] \\
&= -\omega_3\omega_4\left[\cos\theta_4(-\cos\theta_3 + \cos\theta_4) + \sin\theta_4(\sin\theta_4 + \sin\theta_3)\cos\varphi\right]. \qquad \text{(A24)}
\end{aligned}$$

For $\varphi = 0$, we find

$$\begin{aligned}
\mathcal{V}_{12}^{[2]PS}(\varphi = 0) &= -\omega_3\omega_4\left(-\cos\theta_3\cos\theta_4 + \cos^2\theta_4 + \sin^2\theta_4 + \sin\theta_3\sin\theta_4\right) \\
&= -\omega_3\omega_4\left(1 - \cos\theta_+\right) = -\omega^2\left(1 - \cos 2\vartheta\right) = \mathcal{K}\omega^2. \qquad \text{(A25)}
\end{aligned}$$

If we use the same approximations as the scalar case, the second vertex factor is approximated as

$$\mathcal{V}_{12}^{[2]PS} \sim -\omega_3^2\omega_4^2\vartheta^2\{\check{\mathcal{R}} + (\mathcal{R}^{-1} + 1)\cos\varphi\} \equiv -\omega_3^2\omega_4^2\vartheta^2 G(\varphi), \qquad \text{(A26)}$$

with

$$\check{\mathcal{R}} \equiv \frac{1}{2}(\mathcal{R} - \mathcal{R}^{-1}). \qquad \text{(A27)}$$

This is consistent with the approximation of Eq. (A25) for a small $\vartheta$:

$$\mathcal{V}_{12}^{[2]PS}(\varphi = 0) \sim -\omega_3\omega_4\vartheta^2(1 + \hat{\mathcal{R}}). \qquad \text{(A28)}$$

Again by taking the square of the second vertex factor, we then naturally define the factor $\mathcal{F}_S$ for the pseudoscalar case:

$$\mathcal{F}_{1212}^{PS} \equiv \int_0^{2\pi} G^2(\varphi)d\varphi \sim 2\pi\{\check{\mathcal{R}}^2 + \frac{1}{2}(\mathcal{R}^{-1} + 1)^2\}. \qquad \text{(A29)}$$

Let us confirm the relations for the case of $\varphi = 0$ as follows: The ratio of the invariant amplitude of the pseudoscalar case to the scalar case as

$$\frac{\mathcal{M}^{PS}_{1212}(\varphi = 0)}{\mathcal{M}^{SC}_{1122}(\varphi = 0)} = \frac{\mathcal{V}^{[1]PS}_{12}\mathcal{V}^{[2]PS}_{12}}{\mathcal{V}^{[1]SC}_{11}\mathcal{V}^{[2]SC}_{22}} = \frac{-2\sin^2\vartheta\omega^2 \cdot \mathcal{K}\omega^2}{\mathcal{K}\omega^2 \cdot -\mathcal{K}\omega^2} \sim 1 \tag{A30}$$

for a low-mass case with a small $\vartheta$. The other non-vanishing invariant amplitudes are limited to $S = 1111, 2222, 1122, 2211$ for the scalar exchange and $S = 1212, 1221, 2121, 2112$ for the pseudoscalar case. These relations can be confirmed by repeating the routine calculations performed above.

## References


[1] http://lambda.gsfc.nasa.gov/product/map/current/best_params.cfm.
[2] L. Amendola and S. Tsujikawa, *Dark Energy* (Cambridge University Press, Cambridge, UK, 2010).
[3] R. R. Caldwell, R. Dave, and P. J. Steinhardt, Phys. Rev. Lett. **90**, 1582 (1998).
[4] L. Wang, R. R. Caldwell, J. P. Ostriker, and P. J. Steinhardt, Astrophys. J. **530**, 17 (2000).
[5] Y. Fujii and K. Maeda, *The Scalar-Tensor Theory of Gravitation* (Cambridge University Press, Cambridge, UK, 2003).
[6] Y. Fujii, Phys. Lett. B **660**, 87 (2008).
[7] C. Brans and R. H. Dicke, Phys. Rev. **124**, 925 (1961).
[8] Y. Fujii, arXiv:0908.4324 [astro-ph.CO].
[9] Y. Nomura, T. Watari, and T. Yanagida, Phys. Lett. B **484**, 103 (2000).
[10] K. Choi, Phys. Rev. D **62**, 043509 (2000).
[11] J. E. Kim and H. P. Nilles, Phys. Lett. B **553**, 1 (2003).
[12] L. J. Hall, Y. Nomura, and S. J. Oliver, Phys. Rev. Lett. **95**, 141302 (2005).
[13] P. Brax, C. van de Bruck, A. C. Davis, J. Khoury, and A. Weltman, Phys. Rev. D **70**, 123518 (2004).
[14] H. J. de Vega and N. G. Sanchez, arXiv:astro-ph/0701212.
[15] Y. Fujii, Nature Phys. Sci. **234**, 5 (1971).
[16] E. Fischbach and C. Talmadge, *The Search for Non-Newtonian Gravity* (AIP Press, New York, 1998).
[17] Y. Fujii and K. Homma, Prog. Theor. Phys. **126**, 531 (2011).
[18] R. D. Peccei and H. R. Quinn, Phys. Rev. Lett. **38**, 1440 (1977).
[19] J. Jaeckel and A. Ringwald, Annu. Rev. Nucl. Part. Sci. **60**, 405 (2010).
[20] M. P. Hertzberg, M. Tegmark, and F. Wilczek, Phys. Rev. D **78**, 083507 (2008).
[21] O. Wantz and E. P. S. Shellard, Phys. Rev. D **82**, 123508 (2010).
[22] K. Homma, D. Habs, and T. Tajima, Appl. Phys. B **106**, 229 (2012).
[23] A. Yariv, *Optical Electronics in Modern Communications* (Oxford University Press, Oxford, UK, 1997).
[24] R. J. Glauber, Phys. Rev. **131**, 2766 (1963).
[25] S. A. J. Druet and J.-P. E. Taran, Prog. Quantum Electron. **7**, 1 (1981).
[26] F. Moulina and D. Bernard, Opt. Commun. **164**, 137 (1999).
[27] E. Lundström et al., Phys. Rev. Lett. **96**, 083602 (2006).
[28] J. Lundin et al., Phys. Rev. A **74**, 043821 (2006).
[29] D. Bernard et al., Eur. Phys. J. D **10**, 141 (2000).
[30] K. Homma, D. Habs, G. Mourou, H. Ruhl, and T. Tajima, Prog. Theor. Phys. Suppl. **193**, (2012).
[31] http://www.extreme-light-infrastructure.eu/.
[32] http://www.int-zest.com/index.html.
[33] P. Gibbon, *Short Pulse Laser Interactions with Matter: An Introduction* (Imperial College Press, London, 2005).
[34] A. Dupays, E. Masso, J. Redondo, and C. Rizzo, Phys. Rev. Lett. **98**, 131802 (2007).
[35] G. Ruoso et al., Z. Phys. C **56**, 505 (1992).
[36] R. Cameron et al., Phys. Rev. D **47**, 3707 (1993).
[37] M. Fouche et al. (BMV Collab.), Phys. Rev. D **78**, 032013 (2008).
[38] P. Pugnat et al. (OSQAR Collab.), Phys. Rev. D **78**, 092003 (2008).
[39] A. Chou et al. (GammeV T-969 Collab.), Phys. Rev. Lett. **100**, 080402 (2008).
[40] A. Afanasev et al. (LIPSS Collab.), Phys. Rev. Lett. **101**, 120401 (2008).

[41] K. Ehret et al. (ALPS Collab.), Phys. Lett. B **689**, 149 (2010).
[42] S. Moriyama et al., Phys. Lett. B **434**, 147 (1998).
[43] Y. Inoue et al., Phys. Lett. B **536**, 18 (2002).
[44] M. Minowa et al., Phys. Lett. B **668**, 93 (2008).
[45] S. Andriamonje et al. (CAST Collab.), J. Cosmol. Astropart. Phys. **0704**, 010 (2007).
[46] E. Arik et al. (CAST Collab.), J. Cosmol. Astropart. Phys. **0902**, 008 (2009).
[47] E. Arik et al. (CAST Collab.), Phys. Rev. Lett. **107**, 261302 (2011).
[48] S. Asztalos et al., Phys. Rev. D **69**, 011101 (2004).
[49] S. J. Asztalos et al., Phys. Rev. Lett. **104**, 041301 (2010).
[50] K. Nakamura et al. (Particle Data Group), J. Phys. G. **37**, 075021 (2010) and the 2011 partial update for the 2012 edition.
[51] http://www.clf.rl.ac.uk/New+Initiatives/The+Vulcan+10+Petawatt+Project/18344.aspx.
[52] http://www.eli-np.ro/documents/ELI-NP-WhiteBook.pdf.
[53] http://www.extreme-light-infrastructure.eu/pictures/Grand-Challenges-Meeting-Report-id66.pdf.
[54] http://www.ile.osaka-u.ac.jp/zone1/activities/facilities/spec_e.html.
[55] http://www.clf.stfc.ac.uk/Facilities/Vulcan/Vulcan+laser/12250.aspx.
[56] http://www.lle.rochester.edu/omega_facility/omega/.
[57] http://int-zest.com/pdf/le-garrec.pdf.
[58] http://www-lmj.cea.fr/index-en.htm.
[59] https://lasers.llnl.gov.
[60] G. Mourou, N. Fisch, V. M. Malkin, Z. Toroker, E. A. Khazanov, A. M. Sergeev, T. Tajima, and B. Le Garrec, Opt. Commun. **285**, 720 (2012).
[61] https://www.izest.polytechnique.edu/izest-home/ican/ican-94447.kjsp?RF=1332339530225.
[62] T. Tajima and J. Dawson, Phys. Rev. Lett. **43**, 267 (1979).
[63] T. Tajima and K. Homma, Int. J. Mod. Phys. A **27**, 1230027 (2012).
[64] http://www.izest.polytechnique.edu.